Journal of Manufacturing Processes 74 (2022) 88–99

Contents lists available at ScienceDirect

Journal of Manufacturing Processes

journal homepage: www.elsevier.com/locate/manpro

Fabrication of flexible microheater with tunable heating capabilities by direct laser writing and selective electrodeposition

Ye Yang [a,b,d], Songwei Li [c,d], Han Xu [b,d], Yang Xu [b,d], Yong Chen [b,c,d,*]

[a] The College of Information, Mechanical and Electrical Engineering, Shanghai Normal University, Shanghai 200234, China
[b] Epstein Department of Industrial and Systems Engineering, University of Southern California, Los Angeles, CA 90089, USA
[c] Department of Aerospace and Mechanical Engineering, University of Southern California, Los Angeles, CA 90089, USA
[d] Center for Advanced Manufacturing, University of Southern California, Los Angeles, CA 90007, USA

ARTICLE INFO

Keywords:
Microheater
Direct laser writing
3D printing
Selective electrodeposition
Laser-induced graphene

ABSTRACT

Flexible microheaters are useful in a variety of fields, such as portable medical instruments, wearable electronic devices, aircraft, and many more. The microheaters that can provide thermal stimuli in a series of small regions have received considerable attention in recent years. In this work, we present a novel manufacturing process for flexible microheaters with designed heating patterns. Such flexible microheaters with customized heating patterns are fabricated using a hybrid manufacturing process that combines direct laser writing, 3D printing, and selective electrodeposition to control the deposition of graphene and copper on a polyimide film. Based on a given heating pattern, a laser-induced graphene (LIG) structure is utilized as the active heating material, and selectively electrodeposited copper defined by 3D-printed masks is used as the electrode material to connect LIG. The width of the heating line can be as small as 60 μm. The total processing time of a typical 60 mm × 30 mm microheater was within 20 min. When connected to electricity, the fabricated microheaters have tunable heating temperatures at designed heating areas. The heating temperature can reach up to 150 °C. Moreover, the microheaters have shown quick heating and stable thermal performance when subjected to bending, twisting, and folding. Compared with the existing microheater fabrication methods, the newly developed manufacturing process is simple to operate and has the advantages of high accuracy (up to 60 μm heating line width), flexible tunability, and low cost (within $5) compared with other conventional microfabrication methods.

1. Introduction

Flexible microheaters capable of exerting thermal stimuli in small regions are important for applications in wearable electronics, portable medical instruments, and other space-limited heating devices [1–3]. In this study, flexible microheaters with customized heating patterns are fabricated using a hybrid manufacturing process that combines direct laser writing (DLW), three-dimensional (3D) printing, and selective electrodeposition (SED) to control the deposition of graphene and copper on a polyimide (PI) film. Based on a given heating pattern, a laser-induced graphene (LIG) structure is utilized as the active heating material, and selectively electrodeposited copper defined by a 3D-printed mask is used as the electrode material to connect LIG. Fig. 1(c) shows the prototype of a flexible microheater with a designed "USC" pattern. The microheaters with such multi-material composition have accurate heating area, high flexibility, and tunable heating capability.

Flexible microheaters and their fabrication techniques in the previous work can be categorized into two types according to the structures: the wire-based, the foil-based, and other novel microheaters.

(1) The wire-based microheaters transfer heat from the resistive wire to the contact surface. The conductive metal wires functionalize as the heating elements. The wire-based heaters are widely used because of their simplicity, reliability, and versatility [4]. However, it has a high demand for machining and winding fine microscale wires. Specific microfabrication techniques, such as the photolithography, soft lithography, and magnetron sputtering, are required to achieve high accuracy and uniformity. For example, Zhang et al. filled the liquid-metal into micro-channels to generate wires in the width of 200 μm with good electric stability for the wearable microheater. The novel structure consisted of three parallel microchannels, including a heating channel and two ventilating side channels. The micro-channels were fabricated through soft lithography [5]. Rao and Kulkarni created a network made

* Corresponding author at: Epstein Department of Industrial and Systems Engineering, University of Southern California, Los Angeles, CA 90089, USA.
E-mail address: yongchen@usc.edu (Y. Chen).

https://doi.org/10.1016/j.jmapro.2021.11.045
Received 17 May 2021; Received in revised form 2 November 2021; Accepted 21 November 2021

of highly crystalline Au wire on quartz to serve as an effective high-temperature transparent heater. The heater has been fabricated by depositing Au onto a cracked sacrificial template. The wire width was typically 2 μm [6]. Morikawa et al. fabricated the heater-embedded mechanically controllable break junctions (MCBJs) by the photolithography and lift-off techniques for the simultaneous measurements of conductance and thermopower of atomic and molecular wires. The microheaters consisted of Pt coils with a 300 nm line-space geometry, and the local temperature can be controlled via Joule heating through adjusting the voltage [7]. However, the above micromachining methods have high costs and complex operation procedures that are not suitable for scalable production. Moreover, for the wire-based microheaters, the heat dissipation is usually limited by both the diameter of the wire and the relatively poor thermal contact between the wire and the substrate. This is because the cross-sectional shape of the wire is a circle instead of a plane, hence, the contact area of the circle-to-plane surface would be much smaller than the plane-to-plane surface.

(2) Compared to the wire-based microheater, the foil-based flexible microheaters possess higher flexibility in designing the specific heating area pattern and better thermal contact between the electrode pattern and the contact object. The fabrication approaches for the foil-based flexible microheaters include the etched foil process, screen printing, photolithography, wet etching, and lift-off processes, etc. Among them, the etched copper foil technique was the most commonly used and has been commercially applied due to its low cost and scalability. However, it is not appropriate for the machining of microheaters due to their limited accuracy. Therefore, other fabrication techniques with higher accuracy have been investigated. For instance, Ohlander et al. developed novel semi-transparent copper microheaters manufactured by a series of photolithography in a roll-to-roll manner, wet etching, and lift-off processes on polyethylene napthalate (PEN) foil [8]. The lithography technique showed excellent machining accuracy but is limited by its machining cost and efficiency. Liparoti et al. applied flexible poly (amide-imide)-carbon black (PAI-CB) composite films as high-performance microheater foil, which was prepared by a solution/casting technique [9]. Rapolu et al. fabricated the flexible high-performance heaters by adhering positive and negative electrodes to the resistor side of the Kapton foil. Electrode deposition was accomplished by screen printing a conductive paste and the subsequent copper deposition [10]. The foil-based microheaters were dependent on the electrode patterns to provide uniform heating areas. The common geometric patterns of microheaters involve the spiral, honeycomb, S-shape, fan shape, meander, etc. The reason for the complex patterns used in the etched metallic foil technique is that the electric conductivity of metal (such as Cu, Al) is rather high. Thus a large length of the pattern is required to provide the appropriate heating resistance needed by the microheater.

Besides, both novel heating materials and new fabrication techniques were studied to improve the performances of the flexible microheaters. Different types of materials were utilized as the heating elements to enhance the microheaters' performance. Various metallic materials, such as Cu, Al, Ag, Au, Pt, etc., were widely used to form metallic heating films or patterns. Scorzoni et al. chose the Cr/Al/Cr sandwich as the heater material and proposed a 4-wire microheater for lab-on-chip system applications [11,12]. In addition, the emerging carbon-based materials have attracted significant interest for high-performance microheaters. For example, Liu et al. fabricated an addressable carbon-nanotubes (CNTs)-film microheater array used in thermochromic displays with a short thermal response time [13]. Falco et al. demonstrated a cost-effective manufacturing method of flexible and fully printed microheaters using CNTs as the heating element. The microheaters covering an area of 3.2 mm^2 obtained a maximum temperature above 70 °C operating at 9.5 V [14]. Besides CNTs, graphene and its derivatives were also some promising carbon-based materials for high-performance flexible microheaters. Xing et al. presented a graphene oxide-microheater to generate microbubbles photothermally [15]. Yan et al. reported an energy-efficient graphene microheater with a tuning efficiency of 1.07 nm/mW and power consumption per free spectral range of 3.99 mW [16]. Khan et al. demonstrated transparent

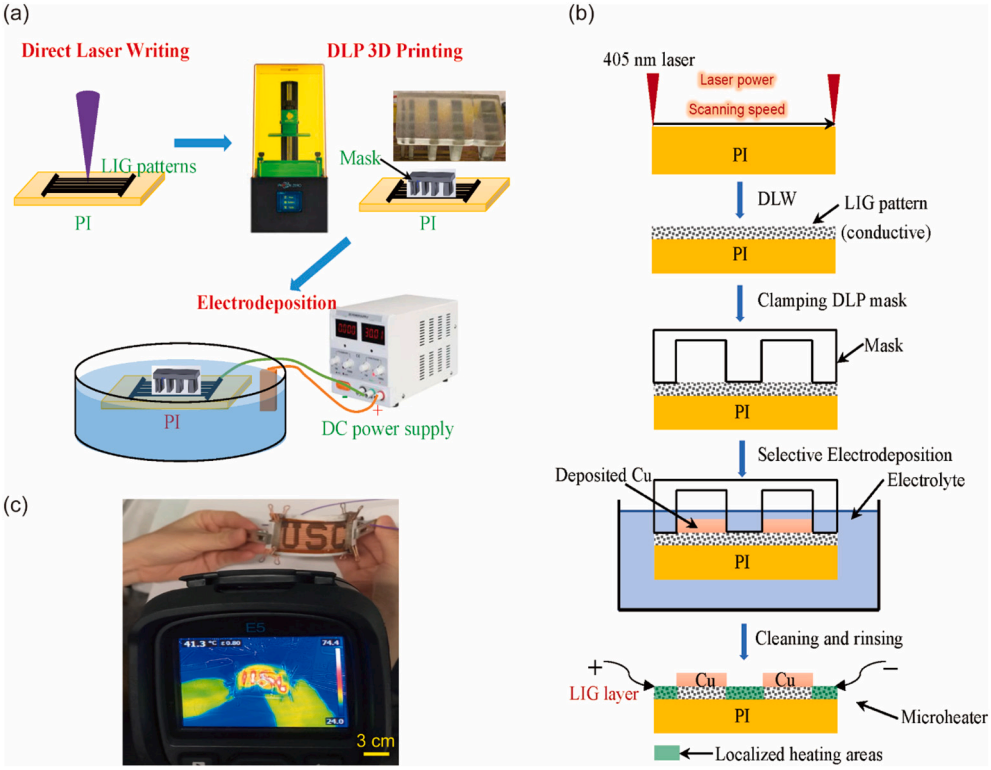

Fig. 1. (a) The schematic diagram for the flexible microheater fabrication. (b) Illustration of the detailed steps to produce the microheaters with multi-material structures. (c) Photo of a flexible microheater designed in the "USC" pattern and its real-time thermal infrared image.

and flexible h-BN passivated graphene microheaters with superior sheet resistance. Moreover, the battery-less, wearable microheaters were powered by a sound-driven textile-based TENG (Triboelectric Nanogenerator). The chemical vapor deposition (CVD) graphene microheaters were fabricated by photolithography [17].

Several novel fabrication approaches, such as DLW and 3D printing, have been rapidly emerged for the scalable and on-demand fabrication of flexible microheaters. The laser-scribing of microheaters has no need for photomasks and complex resist operations. And the DLW method is suitable for microscale applications due to its high machining accuracy and precision. Bobinger et al. fabricated the flexible and robust LIG heaters on bare polyimide substrates through DLW [18]. Wang et al. investigated the electrothermal response and reliability of flexible graphene micro-heaters, which were fabricated using ultrafast laser ablation. Arbitrary patterns were generated for the microheaters by laser writing or scribing [19]. Recently, direct 3D printing was applied in microheater fabrication with low cost and high performance. For instance, Yin et al. printed the microheater with the MWCNTs/PDMS ink solution. The integrated 3D-printed microheater sensor with the drug-encapsulated microneedle system was aimed at pain management [20]. Nevertheless, most microheaters fabricated from the above-reviewed fabrication techniques mainly used a single material such as continuous wire, foil, and LIG patterns. Consequently, the heating films have limited capability of heating separated small areas and overheating control.

In this study, we initiate a strategy of using multi-material composition to obtain the desired temperature at specific sites. A flexible microheater on a PI film consists of graphene and copper, whose electric resistances have over three orders of magnitude difference. Hence, the laser-induced graphene serves as the active heating element while the selectively electrodeposited copper is used as the electrode material to connect the heating element. The heating element can provide the constant localized heating temperature at the designed areas defined as pixels. The heating temperature can be tuned, ranging from the room temperature up to 150 °C. Furthermore, a novel hybrid manufacturing process that combines DLW, 3D printing, and SED has been developed to fabricate the flexible microheaters. Compared with the existing microheater fabrication techniques, this manufacturing process possesses the advantages of high accuracy, simple operation, flexible design, and low cost.

2. Experimental setup and methods

The flexible microheater fabrication process mainly includes the following steps: 1) direct laser writing process to generate the conductive carbonaceous structures on the precursor film surface; 2) digital light processing (DLP) based 3D printing of the covering mask used in the selective electrodeposition; 3) electrodeposition of copper film on the areas without the mask coverage. Fig. 1(a) shows the schematic illustration of the fabrication process. Fig. 1(b) shows a detailed illustration of the steps to produce the multi-material structures for the flexible microheater, composed of the carbonaceous structure and the metallic electrode structure.

Polyimide is a lightweight, flexible material with excellent heat and chemical resistant properties and is widely used in flexible heaters. In this work, the substrate material of PI films was used as the precursor. The PI film substrate provided the microheaters with outstanding flexibility and thermal tolerance. In the experiments, two types of non-adhesive PI films purchased from Sigma-Aldrich in the thickness of 30 μm and 125 μm were applied as the ultrathin film and the common flexible film, respectively. Microheaters made from the ultrathin 30 μm PI films can be attached to the highly curved surfaces easily, while the 125 μm flexible PI films possess higher mechanical strength. The selection of appropriate PI film type depends on the practical applications for the microheaters.

The E-Brite Ultra Cu alkaline non-cyanide electrolyte purchased from EPi Company was used for the electrodeposition of the Cu material. The electrolyte was able to provide the uniform low current density distribution with greater throwing power than cyanide Cu electrolyte. And the non-cyanide electrolyte was much eco-friendly than the electroless plating electrolyte, as shown in the studies of Chen et al. [21] and Ali et al. [22].

The detailed experimental procedures are described as follows:

(1) Firstly, the direct laser writing of the PI films was performed by a laser engraver to generate the desired heating patterns. The machining parameters were listed in Table 1. The 405 nm blue laser was used to pattern the surface of the PI film. The generated carbonaceous structures (carbon black or graphene) depend on the laser power, scanning speed, the number of repetitive scanning passes, and the thickness of PI film. The pattern path was arbitrarily designed by a computer-aided design (CAD) software system. The systematic investigation of the parameter influences on the resulted carbonaceous materials was performed. The appropriate parameters to achieve the graphene material on the modified PI film surface were identified. Compared with the carbon black, the graphene material exhibited a higher electric conductivity and stronger surface adhesion to the intrinsic PI film.

(2) Secondly, the DLP-based 3D printing process was followed after DLW to prepare the covering mask that was used in the next step. Unlike the conventional laser-based stereolithography process, the DLP-based 3D printing uses ultraviolet projection light to photocure liquid resin into layers [23,24]. The *XY* resolution of the DLP 3D printer was around 50 μm. A DLP 3D printer with a higher resolution can also be used [25]. Both rigid and flexible resins were utilized to print the masks. Multi-material DLP-based 3D printers could enable the fabrication of a mask with both rigid and flexible resins [26]. The good surface finish enabled by the DLP-based 3D printing is important to the close contact between the mask and the protected substrate. The flow channels in the mask were designed at the height of 3.0 mm to 10.0 mm, taking the circulation and supplement of the fresh electrolyte flow into consideration.

(3) The third step is the selective electrodeposition (SED) of Cu patterns on the designed regions. The electrodepositing or electroplating of metallic film is superior to electroless plating due to its eco-friendliness, effective thickness control, and smooth surface finish. The selectiveness of the electrodeposition to form the Cu patterns was realized by the assistance of the covering mask. The 3D-printed mask was made from photocurable resins with good insulation. The mask was clamped with the substrate to cover the undeposited regions during the electrodeposition processes. In the previous works of microdevice fabrication by Matsumura et al. [27], Kimura et al. [28], and Seley et al. [29], the electrodeposition followed by the lithography process was performed to obtain the designed patterns. However, the lithography process required complicated operations, and the deposited patterns cannot be removed from the substrate. To achieve the designed patterns' electrodeposition on the carbonaceous substrate, we investigated the simple selective electrodeposition method by clamping the 3D-printed mask on the substrate. The electrodeposition thickness was controlled by the applied voltage amplitude, local current density, and machining time. The suitable electrodeposition parameters for smooth surface finish and high accuracy were studied in this study. The surface of the conductive areas submerged in the electrolyte was uniformly deposited with Cu particles to form the designed Cu patterns. The surface areas covered by the mask were protected from exposure to the electrolyte.

Table 1
Main experimental parameters and their settings in the microheater fabrication.

Procedure	Parameter	Setting	Unit
DLW	Laser power P	10–200	mW
	Scanning speed ν	180–720	mm/min
	Number of scanning passes N	2	/
SED	DC voltage for electrodeposition V	6–10	V
	Electrodeposition time t	10–30	min

Thus, no electrochemical reaction took place in these covered areas. The electrolyte was heated to 50 °C and stirred during the electrodeposition process. The increased temperature and electrolyte circulation could enhance the electrochemical reaction rate. The electrochemical reaction that took place at the cathode is shown as follows:

$$Cu^{2+} + 2e^{-} \rightarrow Cu \quad (1)$$

After the electrodeposition process, the 3D-printed mask can be easily removed from the substrate after removing the clamp. Finally, the fabricated microheater was thoroughly cleaned in deionized water and dried out. Additional PI film or Polydimethylsiloxane (PDMS) can be used to encapsulate the fabricated microheater.

The detailed multi-material structure using the above hybrid fabrication processes is illustrated in Fig. 1(b). The microheaters are composed of polyimide, graphene, and copper. The graphene pattern areas with large resistance are the heating element regions, which can be freely designed according to practical applications. The Cu pattern areas with small resistance serve as the electrode connectors. The PI polymer film substrate provided the flexibility and encapsulation of the microheater devices. The fabricated flexible microheaters have high tunability and heating performance.

3. Experimental results

3.1. The influence of the DLW parameters on the LIG characteristics

We first investigated the effect of various DLW parameters on the LIG structures. Fig. 2 shows the square areas of carbonaceous structures modified by DLW under different power intensities and scanning speeds on the top surface of the PI films in the thickness of 30 μm and 125 μm, respectively. The square structures were all generated under twice scanning passes. It can be observed in Fig. 2(a) for the PI film in the thickness of 125 μm, when the laser power intensity was insufficient, the produced carbonaceous structures tend to become carbon black instead of graphene. The modified carbon black material was easy to fall from the PI substrate surface since the adhesion between carbon black and the PI substrate was rather poor. On the contrary, the LIG material has shown a strong adhesive bond with the intrinsic PI polymer. It has been tested that LIG would not be peeled off from the PI substrate after more than 50 cycles of bending over 90°. Fig. 3(a) shows the optical microscope view of the graphene area. The scanning electron microscope (SEM) images of the typical 3D porous LIG morphology and its interface with the PI film are shown in Fig. 3(b)–(d). The SEM image of the LIG structures after 50 cycles of deformation test is shown in Fig. 3(e). As to the scanning speed, too low scanning speed was time-consuming; however, according to our experimental observations, DLW with a scanning speed too high could only generate carbon black.

Fig. 4 shows the relation of the electrical resistance versus the DLW fabrication parameters. The resistance of the carbonaceous structures varied with the laser power intensity and the scanning speed. The cross symbols in Fig. 4 represent the carbon black materials shedding off from the PI substrates. The much lower laser power intensity was insufficient to produce the continuous and dense LIG structures with low resistance. At the same time, too high laser power also tended to increase the resistance of LIG structures. The high scanning speed of 720 mm/min led to the nonuniform LIG patterns, whose resistance also increased sharply.

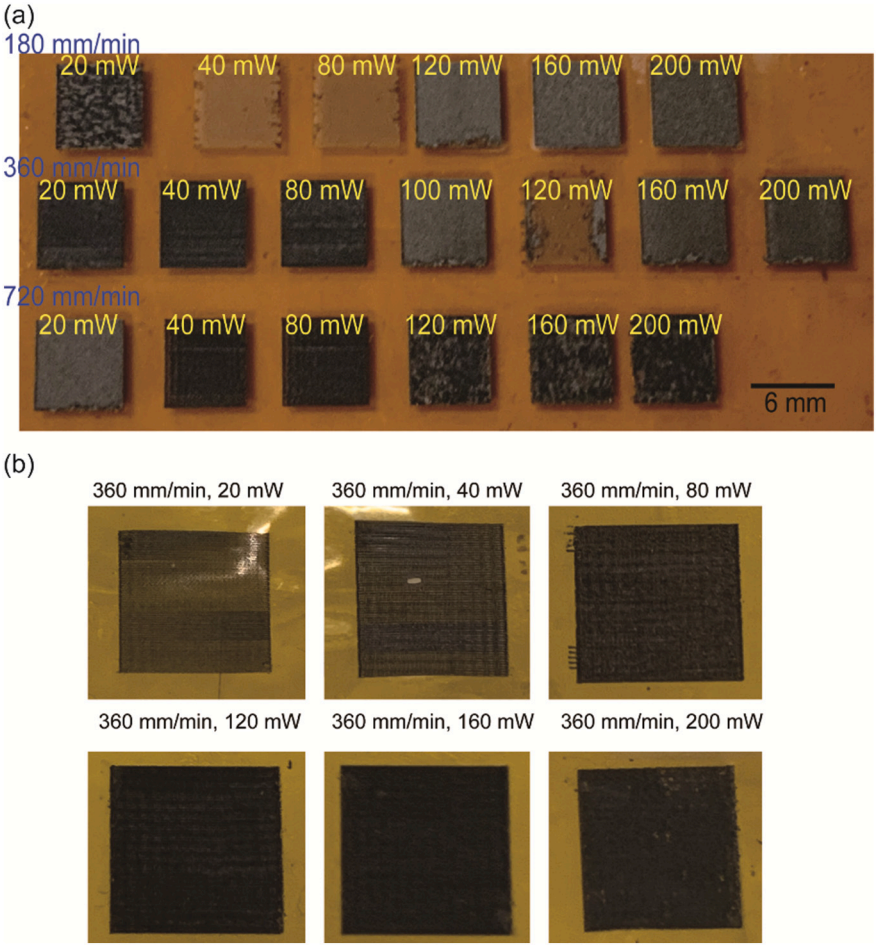

Fig. 2. Photo images of the carbonaceous square patterns scribed under different DLW parameters. (a) On the PI film in the thickness of 125 μm. (b) On the PI film in the thickness of 30 μm.

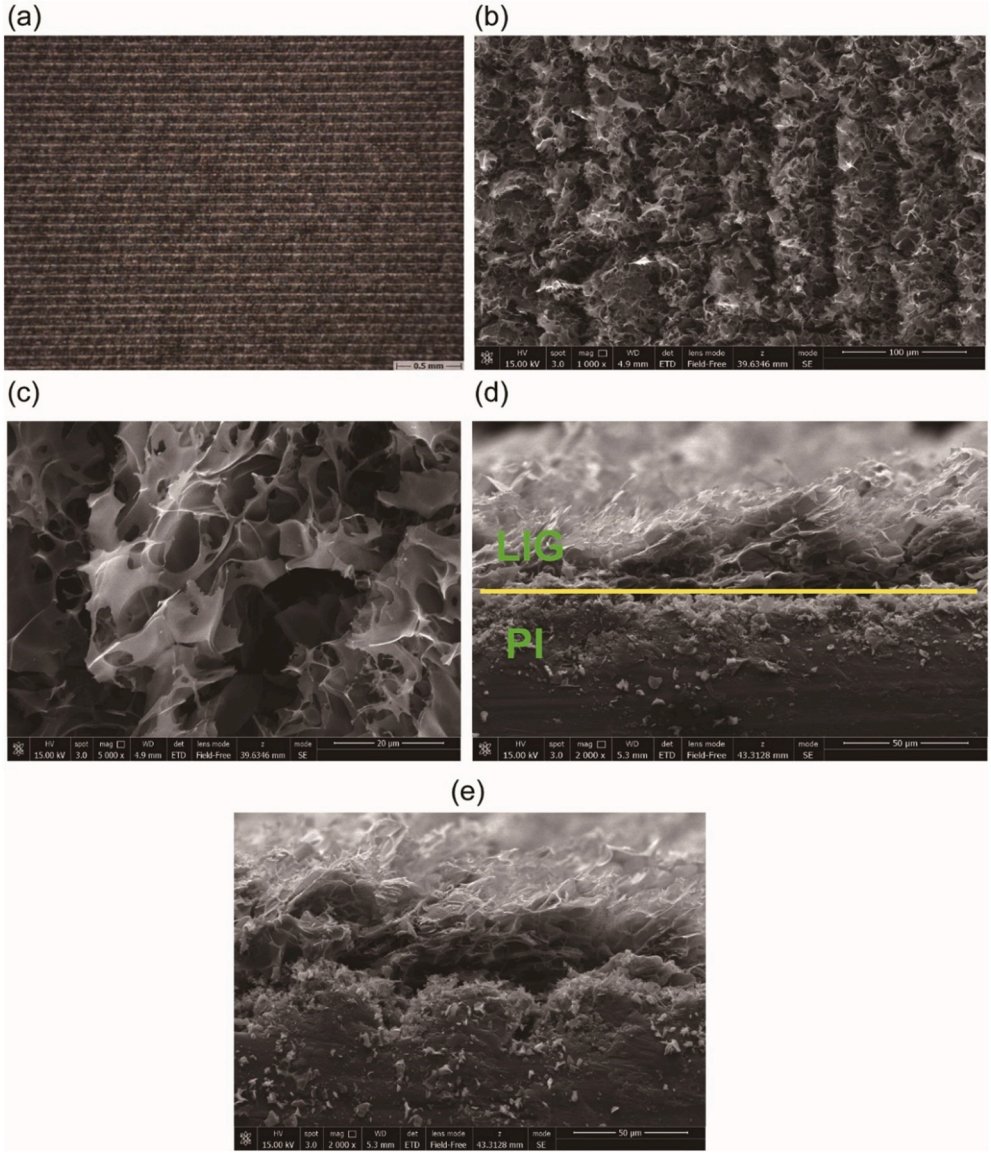

Fig. 3. (a) Optical microscope image of the LIG square area. (b)–(c) Typical SEM images of the LIG in two magnified scales (top view). (d) Typical SEM images of the cross-sectional view of the scribed porous LIG and the PI substrate interface. (e) LIG structures after 50 cycles of deformation test including bending and twisting.

The low scanning speed of 180 mm/min could generate the LIG structures with high electric conductivity when the laser power was above 100 mW; however, a low scanning speed was time-consuming. For the ultrathin PI film in the thickness of 30 μm, similar experimental tendencies were observed, as shown in Fig. 2(b). Therefore, the combination of the scanning speed of 360 mm/min and laser power intensity of 160 mW were chosen to generate the porous LIG with high electric conductivity in the remaining test cases.

Uniform and continuous LIG heating patterns in the fabricated microheaters are critical to ensure their high heating performance. It was observed that the electric conductivity of the porous LIG on the PI film was tunable by applying different combinations of laser power intensity and scanning speed. Also, the tunability of the flexible microheaters could also be realized from the customized heating resistances in the small heating areas designed through the LIG patterns with different widths and lengths, which will be explored and demonstrated in the designed test cases.

3.2. Selective electrodeposition of the Cu patterns

3.2.1. 3D-printed electrodeposition masks

Electrodeposition masks were designed using a CAD system and prepared using the DLP-based stereolithography process for the next step of selective electrodeposition of Cu. The design of the electrodeposition masks considered the following three factors: (1) mask pattern of the heating areas, (2) flow channel of the electrolyte, and (3) the stable clamping sites. The bottom surface of the mask directly contacts the DLW modified PI substrate surface to cover the specific areas from being exposed to the electrolyte. Hence there is no electrochemical reaction at the designed mask pattern areas. Typical masks used for the multiline microheater involving a series of small thermal pixels during the selective electrodeposition are shown in Fig. 5. The bottom patterns of the masks were used to contact the LIG areas to protect them from being electrodeposited. The pillars in the height of 3.0 to 10.0 mm were designed to provide the fluidic channels for the electrolyte circulation. The top plane of the masks was created as the supporting plane for the stable mechanical clamping by an added weight or clips. The 3D printing process provided a simple, fast, and customized approach to fabricate

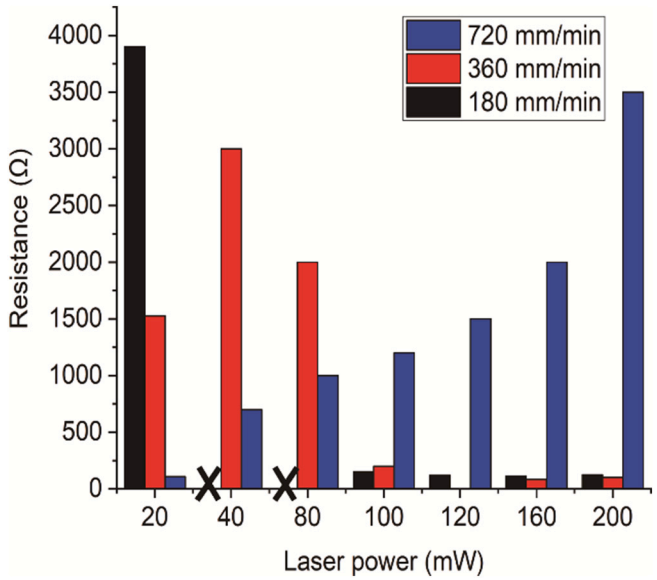

Fig. 4. The measured electric resistance of LIG areas (diagonal line) under different DLW parameters including laser power intensity and scanning speed on the PI films in the thickness of 125 μm.

the insulating masks that can be easily removed afterward. The mask image resolution of the DLP-based 3D printer was ~50 μm. Both rigid and flexible resins were utilized to produce the masks for the following electrodeposition process. Commercial photocurable resins from SprintRay (Los Angeles, California) and PhotoCentric (Peterborough, UK) were used for the rigid masks (Fig. 5(a)–(b)) and flexible masks (Fig. 5(c)), respectively. Both of them can be used as electrodeposition masks.

3.2.2. *The influence of the electrodeposition parameters*

We have investigated the effect of the SED parameters on the metallic Cu pattern deposition on the top of LIG material. The voltage value of the direct current (DC) power supply (V) and the electrodeposition time (t) were crucial to the Cu formation. Fig. 6 shows the electrodeposition on the LIG patterns under different voltage amplitudes and electrodeposition times.

When the voltage was relatively low at 6 V, it took a long time (around 30 min) to form the uniform Cu patterns. A small amount of LIG shedding was observed at the edge. At the voltage of 8 V, uniform and continuous metallic Cu films were gradually formed along the increased electrodeposition time. The surface roughness was obviously reduced. When the voltage was increased to more than 10 V, the electrochemical reaction rate of Cu deposition was increased. However, too intense reaction would cause LIG peeling off from the PI substrate, as seen in Fig. 6(c). Therefore, the selected DC voltage of 8 V and the electrodeposition time of 20 min were applied for the selective electrodeposition for customized microheaters in our study. Fig. 7 shows the approximately linear growth of the thickness of the electrodeposited Cu film on a 30 mm × 30 mm LIG square area with the increasing deposition time at the DC voltage of 8 V.

3.2.3. *The selective electrodeposition of copper patterns by covering mask*

In the following studies, the selective electrodeposition of Cu patterns on the top surface of modified LIG areas was obtained with the assistance of the 3D-printed masks. The flexible PI substrate with the prepared LIG patterns was fixed on a thin glass sheet for clamping together with the mask firmly. The photos of the selective electrodeposition setup are shown in Fig. 8(a). The microheater array pattern fabricated after the selective electrodeposition is shown in Fig. 8(b). The non-porous, fine-grained, smooth, and ductile Cu deposits were produced on the desired micro-areas. Each Cu block was in the size of 0.8 mm × 0.8 mm.

3.3. *Performances of the flexible microheaters*

3.3.1. *Characteristics of the heating capabilities*

Flexible microheaters fabricated by the developed manufacturing process were made on the PI substrate with hybrid LIG and Cu patterns. The heating elements of the microheater were LIG patterns on the flexible PI film surface, while the metallic Cu patterns were used as the electrode material. The heating properties of customized microheaters were studied. Fig. 9 shows the microheater composed of 5 lines in different widths of 0.5 mm, 0.8 mm, 1.2 mm, 1.8 mm, and 2.7 mm, respectively. A 3D-printed mask covered the designed sites of No. 1 to 5 from being exposed to the electrodeposition of Cu. Thus the blue blocks shown in Fig. 9(b) would be retained as LIG material, while the rest black LIG pattern would be deposited by Cu material. The length of the

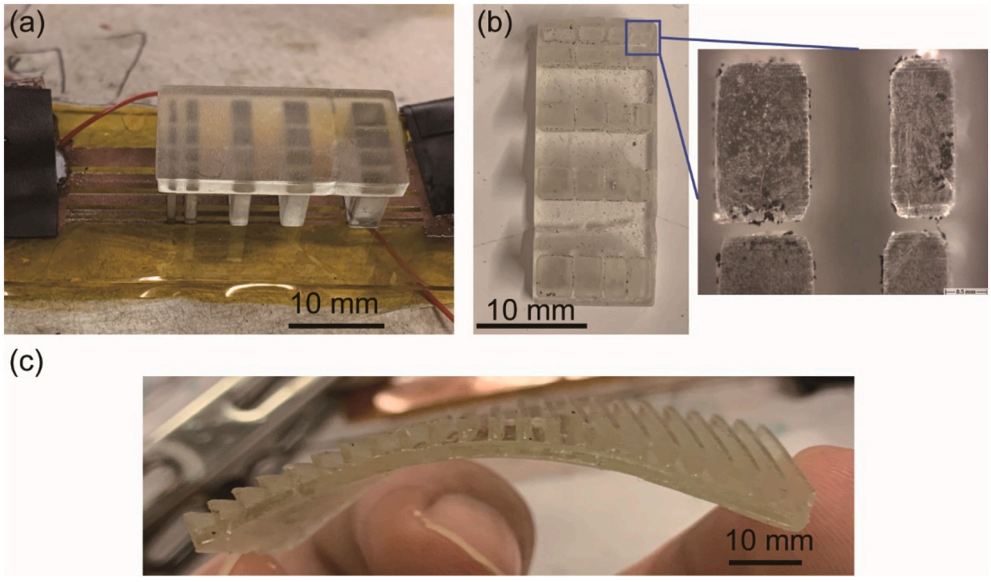

Fig. 5. 3D-printed mask with microscale resolution: (a) Photo of a rigid mask. (b) Optical microscope image of the rigid mask for multi-pixel regions. (c) Photo of a flexible mask for an array microheater.

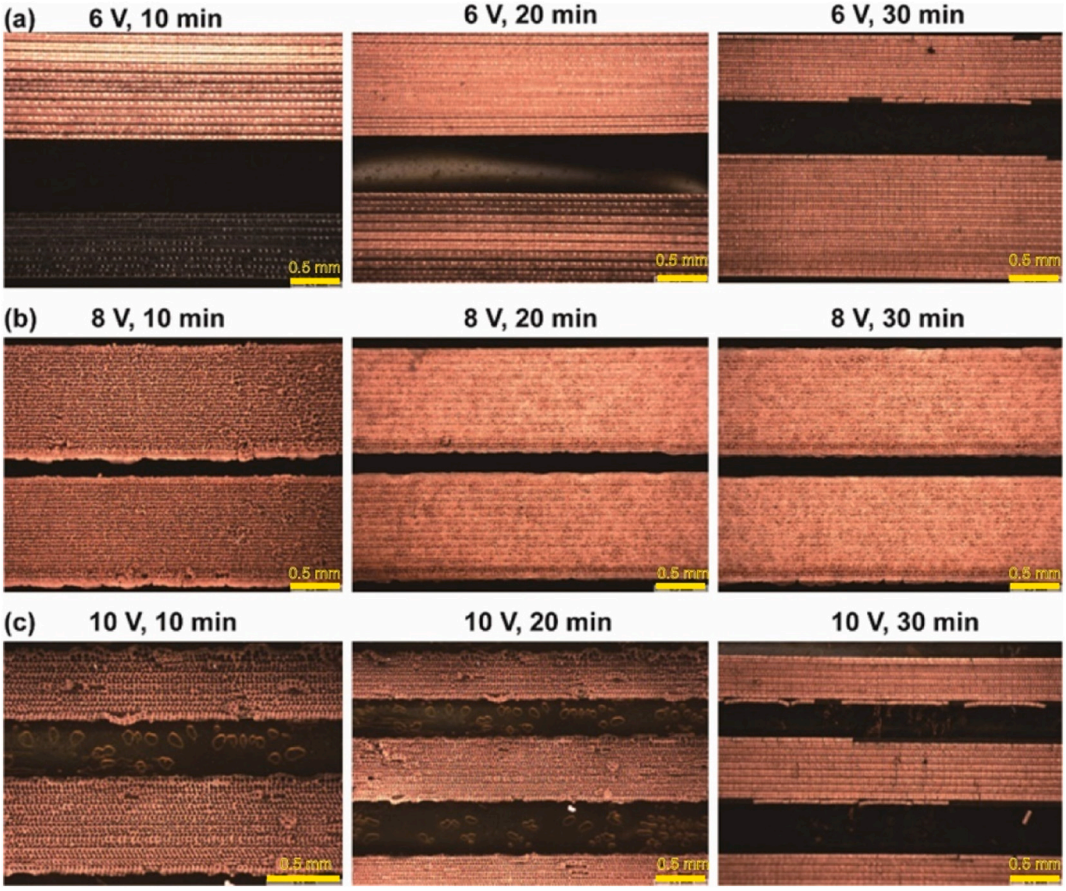

Fig. 6. Electrodeposition of Cu on the LIG multiline patterns under the voltage of (a) 6 V, (b) 8 V, and (c) 10 V, and the electrodeposition time of 10 min, 20 min, and 30 min, respectively.

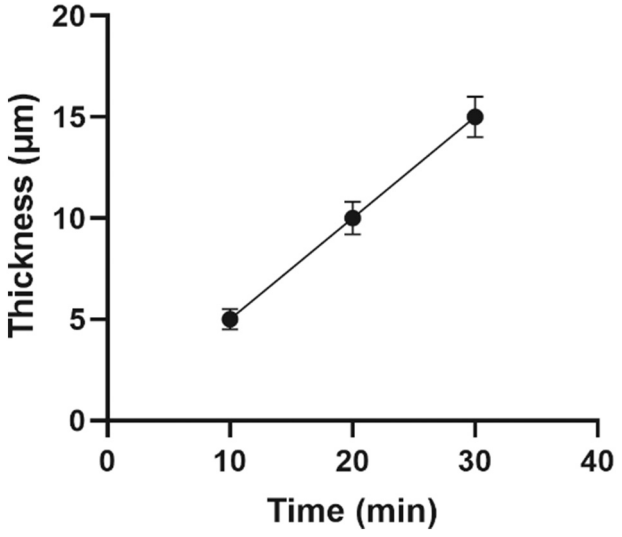

Fig. 7. Thickness of the electrodeposited Cu film versus deposition time.

LIG blocks from sites No. 1 to 5 varied at 1.2 mm, 3.0 mm, 4.0 mm, 5.0 mm, and 6.0 mm, respectively. After the selective electrodeposition with the help of the mask, the fabricated microheater, as shown in Fig. 9(a), was tested under the DC voltage power supply to investigate its heating performances. The resistance of each LIG heating block in different lengths is shown in Fig. 9(c). The electric resistance of the LIG block reduced with the increased width and increased with the increased length of the LIG heating block. Since Joule heating relies on the electric resistance to generate thermal power, the LIG blocks with a larger electric resistance would generate higher heat energy. In addition, the resistance of the deposited Cu pattern was as low as 0.5 Ω to 2 Ω even in the length of 100 mm. Therefore, the Joule heat produced on the electrodeposited Cu pattern was negligible, and the Cu pattern could be regarded as the electrode.

As shown in Fig. 10, the heating performances of a single LIG heating block in the size of 10 mm × 10 mm were measured under different DC voltages. The temperature response was rapid. It needed within 1 min to rise from the room temperature to its maximum temperatures from 40 °C to 120 °C under the voltage from 4.5 V to 11.0 V. When the maximum temperature was reached, the temperature would maintain stable. The rapid heating and stable temperature properties were ideal for microheater applications. The heating temperature for the 10 mm × 10 mm square area could be tuned from the room temperature to approximately 150 °C by the input voltage from 4 V to 30 V. For a smaller heating area with a designed LIG pattern, the maximum temperature would be even higher under the same voltage input. In addition, the repeatability of the microheaters were tested by performing the heating experiments for more than 50 times. The results showed their stable heating performances could maintain with the temperature difference within 5 °C during the 50 times heating and cooling processes.

We further demonstrated the tunability of the flexible microheaters with customized heating patterns. As shown in Fig. 11, a microheater in the pattern of “USC” letters was designed and fabricated using our hybrid fabrication process. The stable temperature distribution of the microheater under 10 V measured by a FLIR thermal infrared imaging camera is displayed in Fig. 11(b). The maximum local temperature at the “USC” pattern rose to 125 °C. And the heating area was constrained at

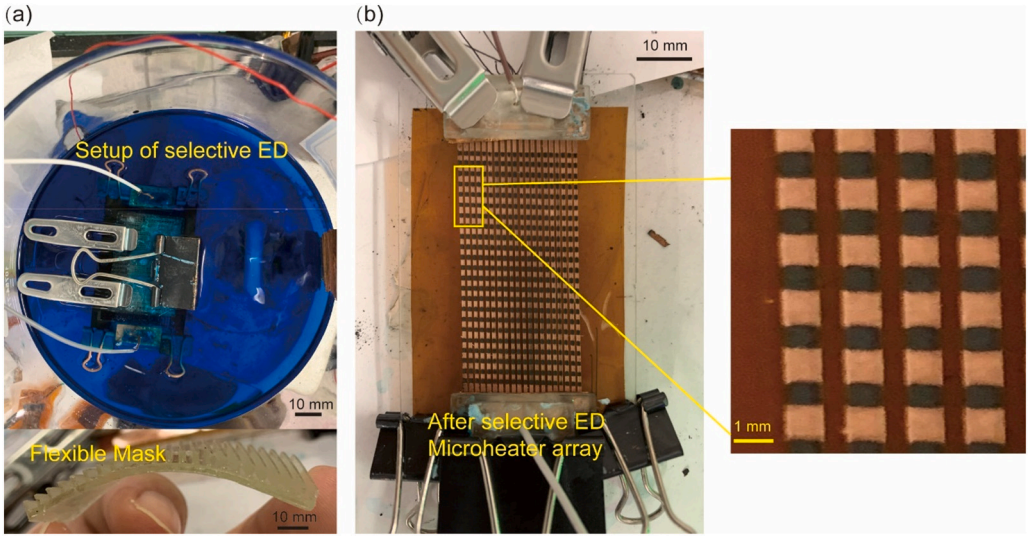

Fig. 8. (a) Photo of the selective electrodeposition setup with the clamped mask. (b) Formation of the Cu pixel array pattern after the selective electrodeposition process.

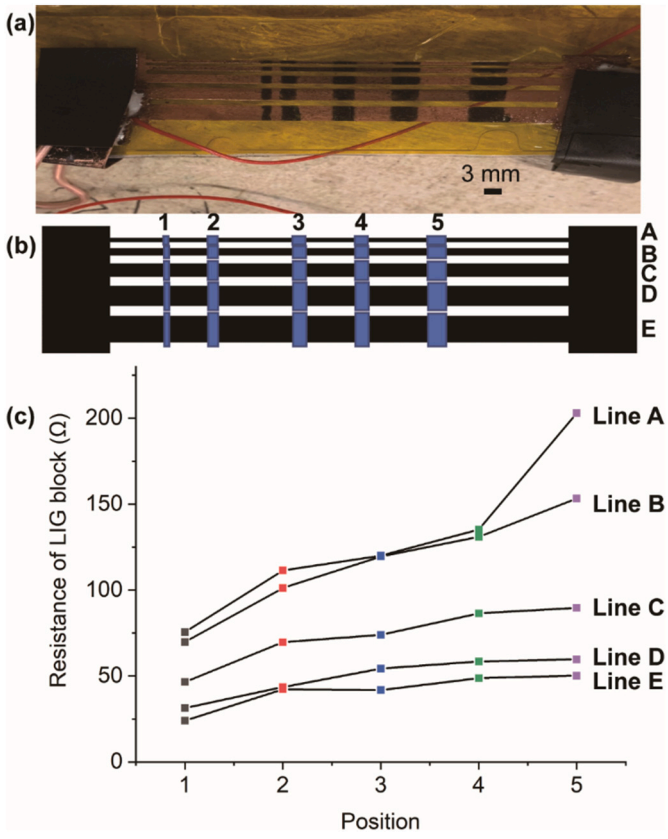

Fig. 9. (a) Photo of a typical multi-pixel microheater. (b) Schematic diagram of the heating pattern at the bottom of the mask on the LIG multi-lines with varying widths. (c) The electrical resistance of the fabricated LIG blocks along the five lines.

the designed pattern region.

3.3.2. *Mechanical flexibility of the microheater*

The mechanical flexibility of the fabricated microheater was investigated through multiple cycles of bending and twisting actions. The heating performances of the microheater during the mechanical bending and twisting were monitored by a FLIR thermal infrared camera. The photos of the microheater's dynamic properties are shown in Fig. 12. Each cycle consists of a bend, an outward twist, and an inward twist. After more than 50 cycles of mechanical testing, the heating performance of the microheater remained stable without any noticeable changes. No cracking or delamination of the Cu and LIG materials were observed, which confirmed the mechanical robustness of the flexible microheater using the developed hybrid manufacturing process. The simple peel tests were conducted by the 3 M Scotch magic tape under the ambient conditions to investigate the adhesion strength between the LIG and the PI substrates. It was observed from the optical microscope that the LIG material remained intact on the PI film after ten-time peels. While for the carbon black structures, only one time peel would strip away most of the particles.

4. Discussions

4.1. *The mechanisms under the hybrid fabrication processes*

In this work, the hybrid fabrication processes based on DLW, 3D printing, and SED were presented to produce flexible microheaters with customized heating patterns. The microheaters were based on the patterned composite material of LIG and Cu on the flexible PI substrate. Therefore, the formation of the LIG pattern and the robust interface between LIG and Cu were crucial. The mechanisms of the related fabrication steps are discussed as follows.

4.1.1. *Formation of the LIG pattern*

The laser-induced graphene prepared by DLW has attracted much attention since its high resolution, cost-effectiveness, and unique 3D porous structures that can be subsequently fabricated into mechanically flexible devices [30–32], graphene-based supercapacitors [33], chemical sensing [34], solar interfacial evaporation [35], etc. Li. et al. demonstrated the high-performance pseudocapacitive micro-supercapacitors (MSCs) from LIG, which exhibited more than two orders of magnitude higher power density than commercial lithium thin-film batteries [36]. Stanford et al. reported flexible electronics beyond the visible limit from LIG with a high spatial resolution of ~12 μm and a thickness of 5 μm. They performed the process in situ in a SEM chamber [37]. Ye. et al. reviewed the LIG from discovery to translation. It is widely believed that the DLW process is scalable, accurate, and flexible [38].

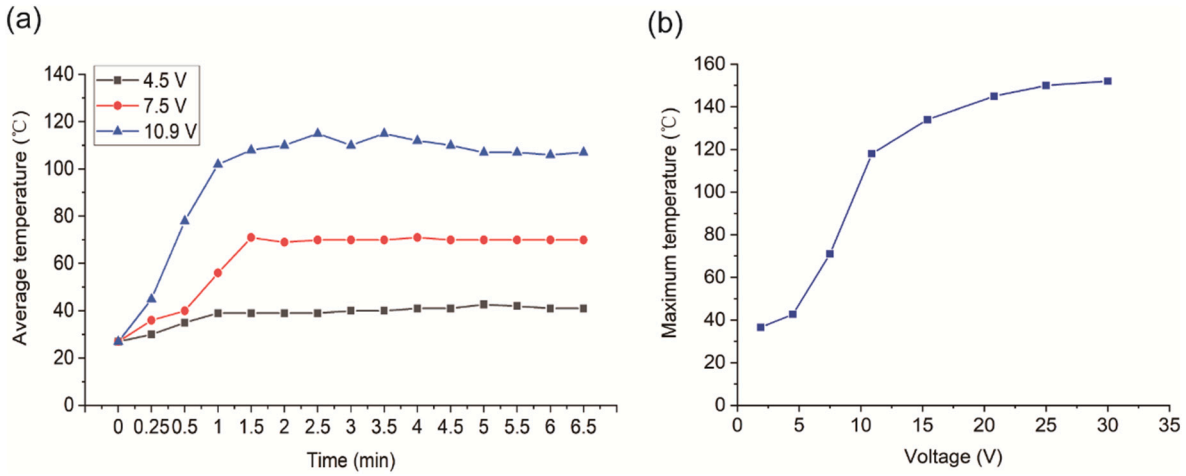

Fig. 10. (a) Temperature vs. heating time under varied DC voltage values for the 10 mm × 10 mm LIG square area. (b) The maximum temperature reached under different voltages.

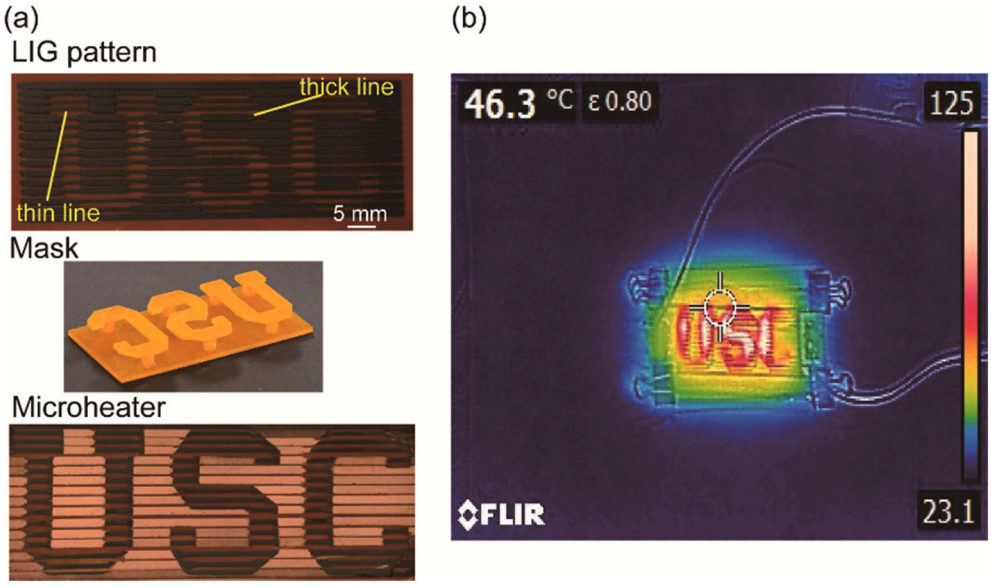

Fig. 11. Demonstration of a flexible microheater with a "USC" pattern. (a) The LIG pattern, 3D-printed mask, and the flexible microheater after the selective Cu electrodeposition. (b) The thermal infrared image of the microheater under 8 V.

It can be observed from Fig. 3(b)–(c), the porous LIG material in this work possessed an accuracy of around 30 μm and a thickness of about 25 μm. The LIG was in a foam-like shape (refer to the SEM image in Fig. 3), which was completely different from the microparticle or granular morphology of carbon black. Therefore, during the peel tests, carbon black structures were easily peeled away by the tape in the particle form, while the graphene structures remained intact after more than 10-time peels. Moreover, from the view of resistance, the resistance of the carbon black structures was rather high since the structures were in particles with no continuous film generated. In comparison, the resistance of the LIG structure was as low as tens to hundreds of ohms since the LIG structures formed the continuous and uniform film on PI substrate. We found that scanning the substrate twice in the moderate laser power and scanning speed could provide repeatable, accurate LIG generation on the PI film surface.

The underlying mechanisms of the LIG structure formation have been systematically studied in the previous work [34,39]. Although the exact mechanism of PI conversion into graphene is still unclear, it is generally regarded that the PI films were utilized as the effective carbon precursors and the photothermal effect of the visible laser was utilized to convert the sp^3 carbon atoms of the precursors to sp^2 carbon atoms. The strong absorption of light in the IR and UV range by PI structure enables photothermal pyrolysis, a high thermal stability and flame retardancy to sustain the localized heating [34].

4.1.2. *Formation of the robust interface*

The selective electrodeposition was achieved by the following two aspects: (1) the designed LIG pattern on the DLW-processed PI surface, and (2) the designed covering mask. The electrodeposited Cu pattern on LIG served as the electrodes. The robust interface between the Cu pattern and LIG pattern was demonstrated by the repetitive deformation of the microheaters, as shown in Fig. 12. The mechanical flexibility and robustness of the interface were obtained by the electrodeposition process. The underlying reason is that the porous and foam-like structures of the LIG material, as seen in Fig. 3(c), provide the connection networks for electrodeposition. Kim et al. found that the increased surface roughness of the polyester (PET) substrate served as the anchor for strengthening the adhesive force between the PET substrate and the

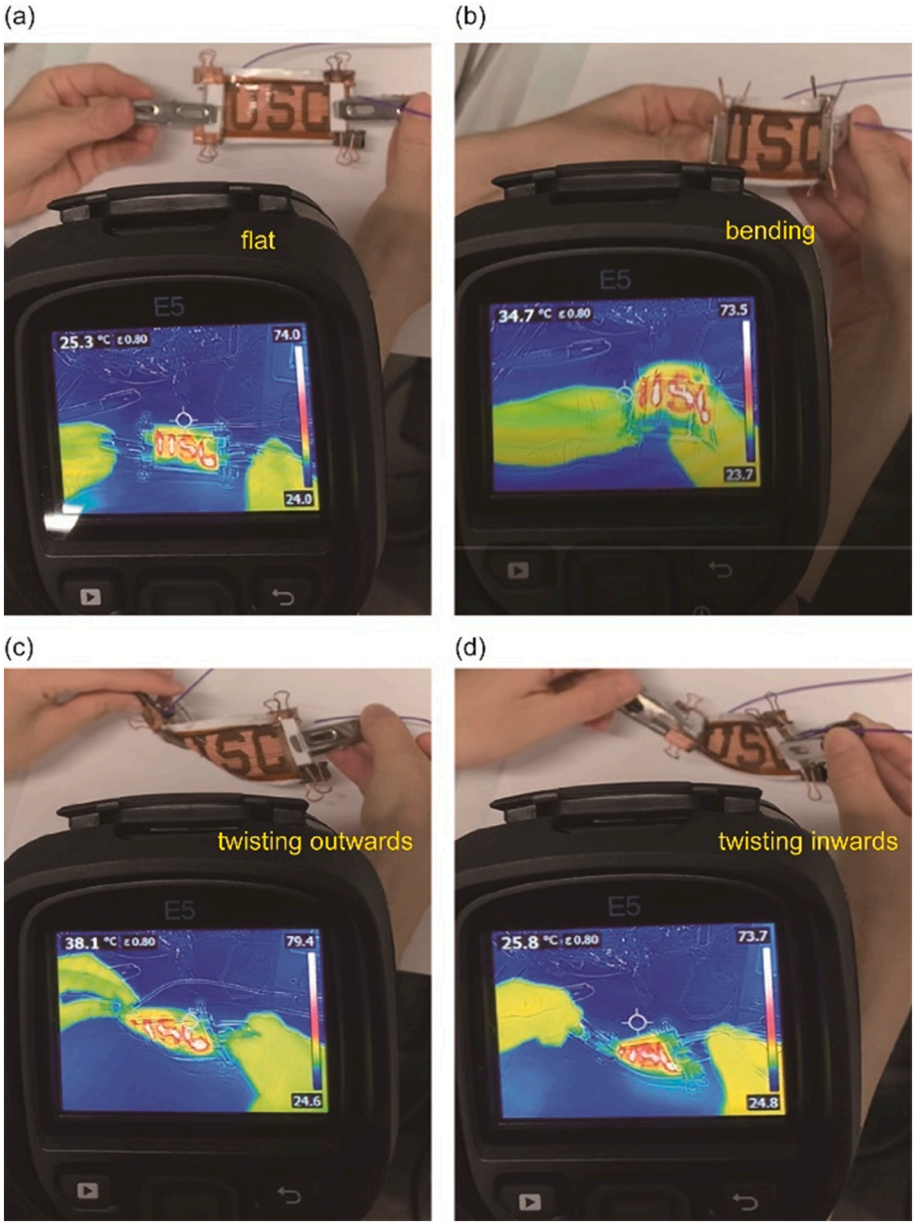

Fig. 12. A cycle for testing the flexibility of the microheater with the "USC" pattern.

overlying Cu layer during the electroless Cu plating [40]. Similarly, in this study, the porous LIG with increased surface roughness can adhere to the electrodeposited Cu films firmly.

The Cu particles initially deposit and intersect with the surface networks of LIG, and then the Cu particles gradually connect to form the continuous Cu film. The time evolution of the Cu deposition is displayed in Fig. 6. Notice the surface roughness of the Cu film would be significantly reduced after the Cu deposition, which is attributed to the self-uniform diffusion of the Cu particles during the electrodeposition process. In our study, both the use of warm electrolyte and the stirred flow of electrolyte promote uniform deposition of Cu on LIG.

4.2. Characteristics of the microheater performances

4.2.1. Tunable heating elements of 3D porous LIG

The electric conductivity of the deposited Cu material was measured and showed over three orders of magnitude higher than that of LIG. Therefore, the material for the active heating areas was the LIG regions on the PI substrates. On the contrary, the selectively deposited Cu pattern areas on LIG served as the electrodes. The heating performances, including thermal response, maximum heating temperature, and heating area, relied on the LIG and Cu pattern combinations, which are highly tunable and free to design.

The Joule heating of the flexible microheaters was achieved from the passage of the current through the continuous conductive pattern. Joule heating can be calculated at a particular location in space according to the following equation:

$$\mathrm{d}P/\mathrm{d}V = J^2/\sigma \tag{2}$$

The power per unit volume $\mathrm{d}P/\mathrm{d}V$ is given by the current density J and the electric conductivity σ. Since the σ of the LIG was tunable by applying different DLW parameters as the experimental results in Fig. 4, the generated Joule heating power and the temperature rise are adjustable. Moreover, the generated heat, Q, is expressed as:

$$Q = I^2Rt \tag{3}$$

where, I is the current flow, R is the resistance, and t is the time of

current flow. The R value is determined not only by σ of the LIG material but also is varied from the width and length of the designed LIG pattern. The tunable performances of the microheater can also be optimized and tailored through the geometric sizes of the customized pattern.

4.2.2. Positive temperature coefficient of the microheaters

From the observation of the thermal performances of the microheaters in Section 3.3.1, we found the microheaters with multi-material composition exhibit a positive temperature coefficient (PTC) characteristic. That is, along with the time evolution, the maximum temperature under the same DC voltage input would be self-limiting, which is crucial to the safety and stability of microheaters. It is suggested that part of the reason may be attributed to the PTC characteristics of Cu material. Moreover, Banerjee et al. presented the printed graphene films on plastic substrates exhibiting metallic type conduction with a PTC of resistance [41]. In this work, the Cu and LIG hybrid patterns on the PI film also have the PTC, which provides high stability for microheaters.

5. Conclusions

A novel manufacturing process to fabricate flexible microheaters with customized heating patterns has been presented. Compared with the existing microheater fabrication methods, the developed manufacturing process was shown viable to fabricate flexible and ultrathin microheaters with arbitrarily designed heating areas with high accuracy and tunable heating performance. The laser-induced graphene patterns were generated on the polyimide film by direct laser writing; then, the electrodeposition masks with designed covering patterns were printed by the DLP-based stereolithography process; finally, the selective electrodeposition of Cu particles was carried out on the LIG areas exposed to the electrolyte. A strong and reliable interface was formed between the LIG layer and the Cu layer. The minimum heating line width reached 60 μm. The total processing time for a typical 60 mm × 30 mm sized microheater was within 20 min. The heating temperature of the fabricated multi-material structure can be tuned by the electric conductivity of LIG and the designed LIG patterns. Based on the measured heating performances, the thermal equilibrium of the microheaters is promptly reached within several minutes. The stable temperature could be maintained for more than several hours when the DC voltage is applied. In addition, the microheater possesses mechanical flexibility and shows heating robustness under bending, twisting, and folding.

The novel microheater manufacturing process opens up a new route for the tunable microheater design, which is promising in various applications that require accurate thermal stimuli in a series of specific surface locations, such as wearable devices, biomedical, microfluidic control, soft robotics, etc. The hybrid electrodeposition process integrated with 3D printing also widens the material selection (e.g., copper, zinc, nickel, etc.) that can be accurately deposited on a multi-material structure.

Declaration of competing interest

The authors declare that they have no known competing financial interests or personal relationships that could have appeared to influence the work reported in this paper.

Acknowledgments

This first author would acknowledge the National Natural Science Foundation of China (Grant No. 51605298) and the China Scholarship Council that supported her to visit the University of Southern California for a year.

References

[1] Kazeminejad H. Thin copper foil heater for measuring the thermal conductivity of polymers. J Appl Polym Sci 2010;88(12):2823–7.
[2] Ryu YK, Carrascoso F, López-Nebreda Rubén, Agrat Nicolás, Castellanos-Gomez A. Microheater actuators as a versatile platform for strain engineering in 2D materials. Nano Lett 2020;20(7):5339–45.
[3] Cao Y, Dong J. High-performance low-voltage soft electrothermal actuator with directly printed micro-heater. Sensors Actuators A Phys 2019;297:111546.
[4] Steinmann RG, Vitoux H. Note: improved wire-wound heater. Rev Sci Inst 2015;86(1):110–31.
[5] Zhang Wang, Li Liu, Gui.. A performance-enhanced liquid metal-based microheater with parallel ventilating side-channels. Micromachines 2020;11(2):133.
[6] Rao KDM, Kulkarni GU. A highly crystalline single Au wire network as a high temperature transparent heater. Nanoscale 2014;6(11):5645–51.
[7] Morikawa T, Arima A, Tsutsui M, Taniguchi M. Thermoelectric voltage measurements of atomic and molecular wires using microheater-embedded mechanically-controllable break junctions. Nanoscale 2014;6.
[8] Ohlander A, Hammerle T, Klink G, Zilio C, Damin F, Chiari M, et al. DNA melting curve analysis on semi-transparent thin film microheater on flexible lab-on-foil substrate. In: 16th International Conference on Miniaturized Systems for Chemistry & Life Sciences; 2012.
[9] Liparoti S, Landi G, Sorrentino A, Speranza V, Cakmak M, Neitzert HC. Flexible poly(amide-imide)-carbon black based microheater with high-temperature capability and an extremely low temperature coefficient. Adv Electron Mater 2016;2(6):1600126.
[10] Rapolu RK, Dugan S, Manelis M, Weldon J, Wessel R, Kapton RS. In: Flexible heaters – design and applications. 2018 17th IEEE intersociety conference on thermal and thermomechanical phenomena in electronic systems (ITherm). San Diego, CA; 2018. p. 19–25.
[11] Scorzoni A, Tavernelli M, Placidi P, Valigi P, Nascetti A. Accurate analog temperature control of a thin film microheater on glass substrate for lab-on-chip applications. In: SENSORS. Valencia: IEEE; 2014. p. 1216–9. 2014.
[12] Scorzoni A, Placidi P, Valigi P, Lovecchio N. Electro-thermal characterization and modeling of a 4-wire microheater for lab-on-chip systems. Applications in electronics pervading industry, environment and society. 2019.
[13] Liu P, Liu L, Jiang K, Fan S. Carbon-nanotube-film microheater on a polyethylene terephthalate substrate and its application in thermochromic displays. Small 2011;7(6):732–6.
[14] Falco A, Romero FJ, Loghin FC, Lyuleeva A, Becherer M, Lugli P, Rivadeneyra A. Printed and flexible microheaters based on carbon nanotubes. Nanomaterials 2020;10(9):1879.
[15] Xing X, Zheng J, Li F, Sun C, Cai X, Zhu D, Chen Z. Dynamic behaviors of approximately ellipsoidal microbubbles photothermally generated by a graphene oxide-microheater. Sci Rep 2014;4(1):1–8.
[16] Yan S, Zhu X, Frandsen LH, Xiao S, Mortensen NA, Dong J, Ding Y. Slow-light-enhanced energy efficiency for graphene microheaters on silicon photonic crystal waveguides. Nat Commun 2017;8(1):1–8.
[17] Khan U, Kim TH, Lee KH, Lee JH, Yoon HJ, Bhatia R, et al. Self-powered transparent flexible graphene microheaters. Nano Energy 2015:356–65.
[18] Bobinger MR, Romero FJ, Salinas-Castillo A, Becherer M, Lugli P, Morales DP, et al. Flexible and robust laser-induced graphene heaters photothermally scribed on bare polyimide substrates. Carbon 2018;144:116–26.
[19] Wang CP, Hsiao MH, Lee GH, Chang TL, Lee YW. The investigation of electrothermal response and reliability of flexible graphene micro-heaters. Microelectron Eng 2020;228:111334.
[20] Yin M, Xiao L, Liu Q, Kwon Sung-Yun, Zhang Y, Sharma PR, et al. 3D printed microheater sensor-integrated, drug-encapsulated microneedle patch system for pain management. Adv Healthc Mater 2019;8.
[21] Chen JJ, Lin GQ, Wang Y, Sowade E, Baumann RR, Feng ZS. Fabrication of conductive copper patterns using reactive inkjet printing followed by two-step electroless plating. Appl Surf Sci 2017;396:202–7.
[22] Ali A, Baheti V, Vik M, Militky J. Copper electroless plating of cotton fabrics after surface activation with deposition of silver and copper nanoparticles. J Phys Chem Solid 2020;137:109181.
[23] Pan Y, Zhou C, Chen Y. A fast mask projection stereolithography process for fabricating digital models in minutes. J Manuf Sci Eng 2012;134:051011.
[24] Pan Y, Chen Y, Yu Z. Fast mask image projection based micro-stereolithography process for complex geometry. J Micro Nano-Manuf 2017;5:014501.
[25] Jia W, Leung Y, Mao H, Xu H, Zhou C, Chen Y. Hybrid-light-source stereolithography for fabricating macro-objects with micro-textures. J Manuf Sci Eng 2022;144(3):031003.
[26] Mao H, Jia W, Leung Y, Jin J, Chen Y. Multi-material stereolithography using curing-on-demand printheads. Rapid Prototyp J 2021;27(5):861–71.
[27] Matsumura Y, Enomoto Y, Tsuruoka T, Akamatsu K, Nawafune H. Fabrication of copper damascene patterns on polyimide using direct metallization on trench templates generated by imprint lithography. Langmuir 2010;26(14):12448–54.
[28] Kimura Y, Fuziwara R, Tsuruoka T, Takashima Y, Nawafune H, Yanagimoto H, et al. Direct fabrication of metal patterns on resin substrate by combining imprint and electrochemical lithography. J Surf Finish Soc Jpn 2016;66(1):18–9.
[29] Seley DB, Dissing DA, Sumant AV, Divan R, Miller S, Auciello O, Hamilton JP. Electroplate and lift lithography for patterned micro/nanowires using ultrananocrystalline diamond (UNCD) as a reusable template. ACS Appl Mater Interfaces 2011;3(4):925–30.
[30] Guo CF, Ding L. Integration of soft electronics and biotissues. The Innovation 2021;2(1).

[31] You R, Liu YQ, Hao YL, Han DD, Zhang YL, You Z. Laser fabrication of graphene-based flexible electronics. Adv Mater 2020;32(15):1901981.
[32] Carvalho AF, Kulyk B, Fernandes AJ, Fortunato E, Costa FM. A review on the applications of graphene in mechanical transduction. Adv Mater 2021;2101326.
[33] Fu XY, Chen ZD, Han DD, Zhang YL, Xia H, Sun HB. Laser fabrication of graphene-based supercapacitors. Photon Res 2020;8(4):577–88.
[34] Vivaldi FM, Dallinger A, Bonini A, Poma N, Sembranti L, Biagini D, Di Francesco F. Three-dimensional (3D) laser-induced graphene: structure, properties, and application to chemical sensing. ACS Appl Mater Interfaces 2021;13(26):30245–60.
[35] Han DD, Chen ZD, Li JC, Mao JW, Jiao ZZ, Wang W, Sun HB. Airflow enhanced solar evaporation based on Janus graphene membranes with stable interfacial floatability. ACS Appl Mater Interfaces 2020;12(22):25435–43.
[36] Li L, Zhang J, Peng Z, Li Y, Gao C, Ji Y, et al. High-performance pseudocapacitive microsupercapacitors from laser-induced graphene. Adv Mater 2016;28(5):838–45.
[37] Stanford MG, Zhang C, Fowlkes JD, Hoffman A, Ivanov IN, Rack PD, Tour JM. High-resolution laser-induced graphene. Flexible electronics beyond the visible limit. ACS Appl Mater Interfaces 2020;12(9):10902–7.
[38] Ye R, James DK, Tour JM. Laser-induced graphene: from discovery to translation. Adv Mater 2019;31(1):1803621.
[39] Liu YQ, Zhang YL, Liu Y, Jiang HB, Han DD, Han B, Sun HB. Surface and interface engineering of graphene oxide films by controllable photoreduction. Chem Rec 2016;16(3):1244–55.
[40] Kim BJ, Park JS, Yoo R, Park JS. Flexible grid-mesh electrodes fabricated by electroless copper plating on corona-treated PET substrates and coating with graphene for transparent film heaters. RSC Adv 2017;7(83):53025–31.
[41] Banerjee I, Faris T, Stoeva Z, Sharma AK, Ray AK. Printed graphene films with positive temperature coefficient of resistivity. Mater Today Proc 2016;3(2016):4035–9.